AD-A193 218 A THREE-DIMENSIONAL MODEL OF THE GAS-CELL ATOMIC FREQUENCY STANDARD..(U) AEROSPACE CORP EL SEGUNDO CA CHEMISTRY AND PHYSICS LAB J C CAMPARO ET AL. 25 FEB 88 1/1

UNCLASSIFIED TR-0086A(2945-05)-2 SD-TR-88-41 F/G 20/3 NL

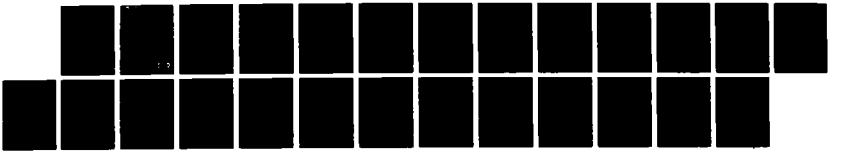

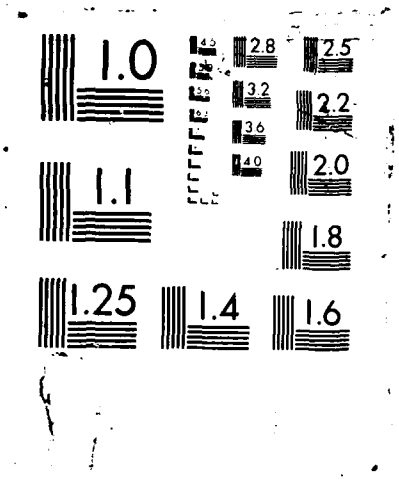
1.0
1.1
1.25
1.4
1.6
1.8
2.0
2.2
2.5
2.8
3.2
3.6
4.0

REPORT SD-TR-88-41

(4)

A Three-Dimensional Model of the Gas-Cell Atomic Frequency Standard

J. C. CAMPARO and R. P. FRUEHOLZ
Chemistry and Physics Laboratory
Laboratory Operations
The Aerospace Corporation
El Segundo, CA 90245-4691

25 February 1988

Prepared for

SPACE DIVISION
AIR FORCE SYSTEMS COMMAND
Los Angeles Air Force Base
P.O. Box 92960, Worldway Postal Center
Los Angeles, CA 90009-2960

This report was submitted by The Aerospace Corporation, El Segundo, CA 90245, under Contract No. F04701-85-C-0086-P00016 with the Space Division, P.O. Box 92960, Worldway Postal Center, Los Angeles, CA 90009-2960. It was reviewed and approved for The Aerospace Corporation by S. Feuerstein, Director, Chemistry and Physics Laboratory.

Lt Michael J. Mitchell was the project officer for the Mission-Oriented Investigation and Experimentation (MOIE) Program.

This report has been reviewed by the Public Affairs Office (PAS) and is releasable to the National Technical Information Service (NTIS). At NTIS, it will be available to the general public, including foreign nationals.

This technical report has been reviewed and is approved for publication. Publication of this report does not constitute Air Force approval of the report's findings or conclusions. It is published only for the exchange and stimulation of ideas.

Michael J Mitchell

MICHAEL J. MITCHELL, Lt, USAF
MOIE Project Officer
SD/CWNZS

Raymond M Leong

RAYMOND M. LEONG, Major, USAF
Deputy Director, AFSTC West Coast Office
AFSTC/WCO OL-AB

UNCLASSIFIED
SECURITY CLASSIFICATION OF THIS PAGE

REPORT DOCUMENTATION PAGE

1a REPORT SECURITY CLASSIFICATION Unclassified	1b RESTRICTIVE MARKINGS
2a SECURITY CLASSIFICATION AUTHORITY	3 DISTRIBUTION / AVAILABILITY OF REPORT Approved for public release; distribution unlimited.
2b DECLASSIFICATION / DOWNGRADING SCHEDULE	
4 PERFORMING ORGANIZATION REPORT NUMBER(S) TR-0086A(2945-05)-2	5 MONITORING ORGANIZATION REPORT NUMBER(S) SD-TR-88-41
6a NAME OF PERFORMING ORGANIZATION The Aerospace Corporation Laboratory Operations 6b OFFICE SYMBOL (If applicable)	7a NAME OF MONITORING ORGANIZATION Space Division
6c ADDRESS (City, State, and ZIP Code) El Segundo, CA 90245	7b ADDRESS (City, State, and ZIP Code) Los Angeles Air Force Base Los Angeles, CA 90009-2960
8a NAME OF FUNDING / SPONSORING ORGANIZATION 8b OFFICE SYMBOL (If applicable)	9 PROCUREMENT INSTRUMENT IDENTIFICATION NUMBER F04701-85-C-0086-P00016
8c ADDRESS (City, State, and ZIP Code)	10 SOURCE OF FUNDING NUMBERS PROGRAM ELEMENT NO / PROJECT NO / TASK NO / WORK UNIT ACCESSION NO

11 TITLE (Include Security Classification)
A Three-Dimensional Model of the Gas-Cell Atomic Frequency Standard

12 PERSONAL AUTHOR(S)
Camparo, James C., and Frueholz, Robert P.

13a TYPE OF REPORT	13b TIME COVERED FROM ____ TO ____	14 DATE OF REPORT (Year, Month, Day)	15 PAGE COUNT
		1988 February 25	24

16 SUPPLEMENTARY NOTATION

17 COSATI CODES			18 SUBJECT TERMS (Continue on reverse if necessary and identify by block number)
FIELD	GROUP	SUB-GROUP	Atomic Clocks, Rubidium Frequency Standard, Noise Processes

19 ABSTRACT (Continue on reverse if necessary and identify by block number)

Preliminary calculations from a three-dimensional clock model are discussed. In particular, a recent conclusion that short-term stability might be improved by varying the microwave power is considered. Results support the general conclusion, but show that the degree of sensitivity is less than predicted by a one-dimensional model. The difference in the results of the two models is a manifestation of the more accurate treatment of the position-shift effect in the three-dimensional model. This more accurate treatment is highlighted by the three-dimensional model's determination of isoefficiency contours (contours showing spatial regions in the clock cavity that have equal efficiency for producing clock signal), and noting their spatial dependence upon microwave power.

20 DISTRIBUTION / AVAILABILITY OF ABSTRACT	21 ABSTRACT SECURITY CLASSIFICATION
☒ UNCLASSIFIED/UNLIMITED ☐ SAME AS RPT ☐ DTIC USERS	Unclassified
22a NAME OF RESPONSIBLE INDIVIDUAL	22b TELEPHONE (Include Area Code) / 22c OFFICE SYMBOL

DD FORM 1473, 84 MAR 83 APR edition may be used until exhausted
All other editions are obsolete

SECURITY CLASSIFICATION OF THIS PAGE
UNCLASSIFIED

CONTENTS

FIGURES

TABLES

I. INTRODUCTION

Over the past few years a one-dimensional, nonempirical model of the gas-cell atomic frequency standard has been developed at The Aerospace Corporation [1]. This model analyzes the servo control feedback circuitry and the signal lineshape of the atomic physics package in order to yield the expected frequency stability of the atomic standard design under study. The model is one-dimensional in that it only considers axial variations in: (a) the clock cavity's microwave magnetic field strength, and (b) the degree of optical pumping within the clock's rubidium (Rb) resonance cell. However, even with this dimensional limitation, the model has been quite useful for analyzing potential frequency stability improvements resulting from the use of a diode laser as the optical pumping light source [2], and also for comparing the potential frequency stabilities of gas cell standards based on alkalies other than Rb [3]. In essence, the one-dimensional clock model has been adequate for addressing these questions because, in these cases, it is reasonable to consider the various spatially varying quantities as averages over the clock cavity's and cell's transverse dimensions.

A one-dimensional model, however, is only marginally adequate for analyzing a wider range of questions concerning Rb clock performance; particularly the potential mechanisms of frequency drift. Specifically, it has been suggested that frequency drift in the Rb standard may result from a spatial motion of the small region of vapor in the clock cavity that gives rise to the major portion of the clock signal [4]. Consequently, an analysis that averaged various quantities over the transverse dimensions of the clock cavity and resonance cell would be unable to investigate this hypothesis. A three-dimensional model of the gas-cell atomic frequency standard is, therefore, required in order to properly examine the plausiblity of this "position shift" mechanism as a contributor to frequency drift.

II. THREE-DIMENSIONAL MODEL

To create a three-dimensional model of the gas-cell atomic frequency standard, we consider the clock cavity to be composed of hundreds of tubes (minimally 6400) as shown in Fig. 1a, each of which can be described by our one-dimensional model; at present we consider only cylindrical TE_{011} and TE_{111} microwave cavity modes, though other spatial configurations could be modeled without much difficulty. As shown in Fig. 1b the transverse distribution of hyperfine polarization is approximated by considering only the first-order radial diffusion mode [5], and tnis is included in the model by superimposing this distribution on the microscopic solutions as previously discussed [1]; for simplicity we have assumed in all calculations that the optical pumping light is uniform in the transverse dimensions. Since diffusional relaxation is now included in the calculations by considering the full three-dimensional hyperfine polarization distribution that results from this relaxation mechanism, phenomenological diffusional relaxation rates are no longer required in the microscopic calculations [1]. For each tube, the normalized stimulating microwave magnetic field, which corresponds to a normalized microwave Rabi frequency, is determined by the transverse position of the tube in the cavity and the cavity mode under consideration (see Fig. 1b). The normalizing constant is determined by the cavity Q and the microwave power fed into the cavity mode. Consequently, the dependence of the clock signal on microwave field strength is expressed simply in terms of: (a) the cavity mode, (b) the cavity Q, and, (c) the input microwave power.

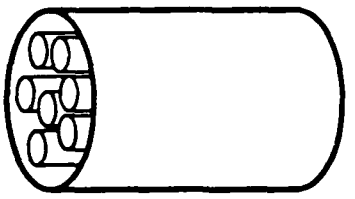

(a)

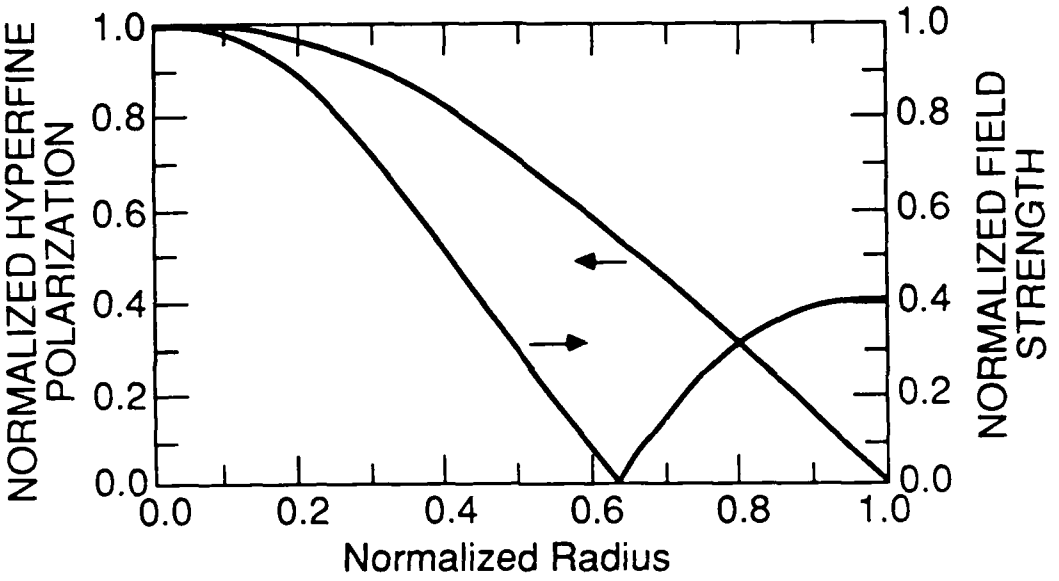

(b)

Fig. 1. Construction of Three-Dimensional Model of the Gas-Cell Atomic Clock. In (a) we imagine the resonance cell as being composed of hundreds of tubes, each of which can be described by a one-dimensional clock model. In (b) we show the radial distributions of both the hyperfine polarization and the absolute value of the microwave magnetic field for a TE_{011} cavity mode. The radial distribution of hyperfine polarization results from diffusional relaxation, and we consider only the first-order radial diffusion mode. The cusp in the microwave magnetic-field strength corresponds to a 180-deg phase shift in the field.

III. DEPENDENCE OF SHORT-TERM STABILITY ON MICROWAVE POWER

Recent studies [1,6] have treated the dependence of the Rb clock's short-term stability on microwave power. In particular, previous calculations have shown that for clock designs similar to that of Williams et al. [7], which are well described by a one-dimensional clock model, the short-term stability of the standard should be a fairly sensitive function of the microwave power P fed into the clock cavity [1]. Qualitatively, this can be understood from the fact that the short-term stability of the standard is shot noise limited [8], which allows writing

$$\sigma_y \sim \frac{\Delta\nu}{S} . \tag{1}$$

Here, σ_y is the square root of the Allan variance (henceforth referred to as the Allan deviation), $\Delta\nu$ is the full widtn of the atomic hyperfine resonance, and S is the atomic resonance signal amplitude. For a single atom or, equivalently, an ensemble of atoms all experiencing the same microwave magnetic field strength (a clock cavity with no spatial field variation), relatively simple expressions relating signal amplitude and width to microwave power may be derived [9]. Considering first the regime of low microwave power (below saturation), S increases linearly with the microwave power and $\Delta\nu$ is constant. Thus, in this regime the Allan deviation is inversely proportional to P. However, in the regime of high microwave power (saturation regime) S is constant and $\Delta\nu$ increases as the square root of the microwave power. Evidence indicates that gas-cell clocks tend to be operated in the saturation regime [10], and one would expect that for clock cavities exhibiting relatively little spatial variation of the microwave field,

$$\sigma_y \sim P^{0.5} . \tag{2}$$

Consequently, if a clock's normal operating point was at a microwave power level well into the saturation regime, then improvement in the short-term stability of the clock could be attained by simply reducing the microwave power to the level corresponding to the onset of saturation.

Typical clock cavities, however, have fields which show considerable variation over the cavity volume. Consequently, since the atoms are effectively frozen in place by the buffer gas during the time intervals over which the clock signal is generated [11], atoms in different regions of the clock's cavity experience different levels of microwave field strength, depending on the clock's cavity mode. This implies that atoms in different regions of the cavity reach the saturation regime at different levels of microwave cavity input power. Since the clock signal is essentially a sum over all of the individual atomic signals, the clock signal can be expected to have a fairly complicated dependence on the microwave power fed into the cavity.

An example of this dependence as predicted by our three-dimensional clock model is presented in Fig. 2, which shows the Allan deviation at 1 sec as a function of microwave cavity input power. In this example we have considered a minimum volume, cylindrical TE_{011} cavity with a Q of 100; other parameters used in the calculations of this paper are collected in Table I.

Table I. Miscellaneous Parameters Used in Clock Model Calculations. See Ref. 1.

Parameter	Value
Optical linewidth	2.0 GHz
Cell temperature	60° C
Photocell response	0.5 A/W
Cavity Q	100
Optical power (D_1)	47μW
Optical power (D_2)	75μW

Additionally, Figs. 3a and 3b show the theoretical clock signal amplitudes and full widths, respectively, as a function of microwave power for this same case. Curves similar to those shown were obtained for the TE_{011} cavity for various optical pumping light intensities and resonance cell temperatures.

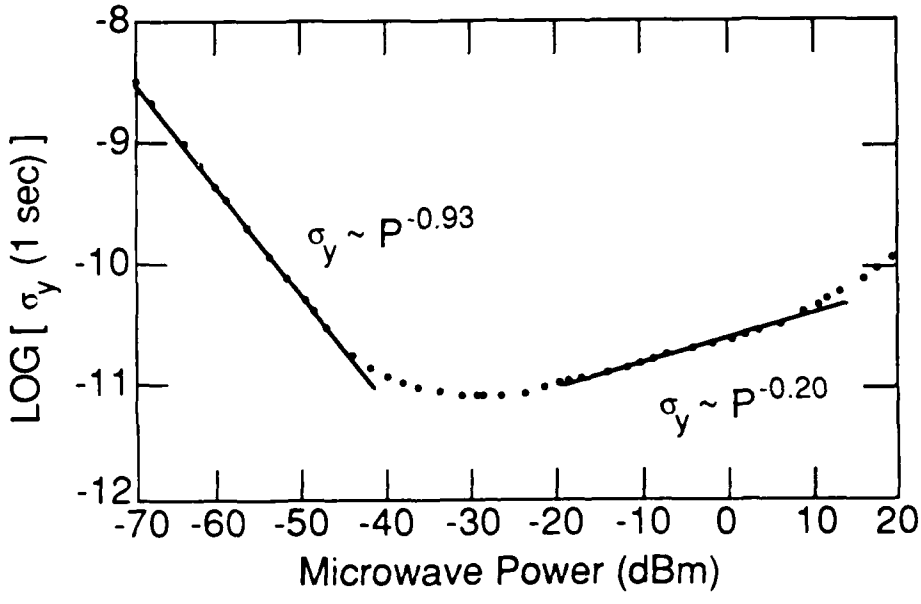

Fig. 2. Log of Allan Deviation as a Function of Microwave Cavity Input Power. For a TE_{011} cavity mode (Q = 100) for both low and high microwave powers, the numerical data are fit to a power law to determine the coefficients shown in the figure. Note that at the highest microwave power (roughly 10 dBm) there seems to be a break in the power-law scaling; a possible explanation for this effect is suggested in the text.

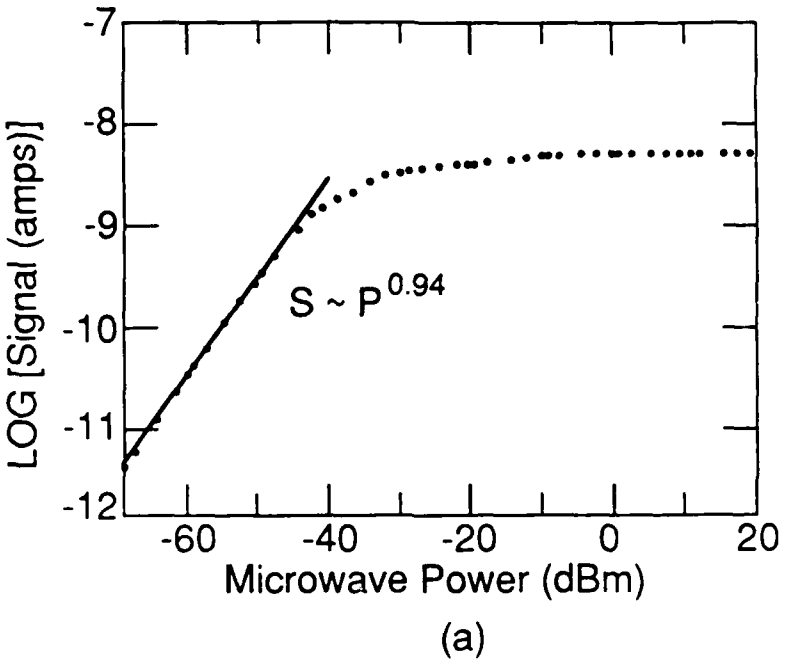

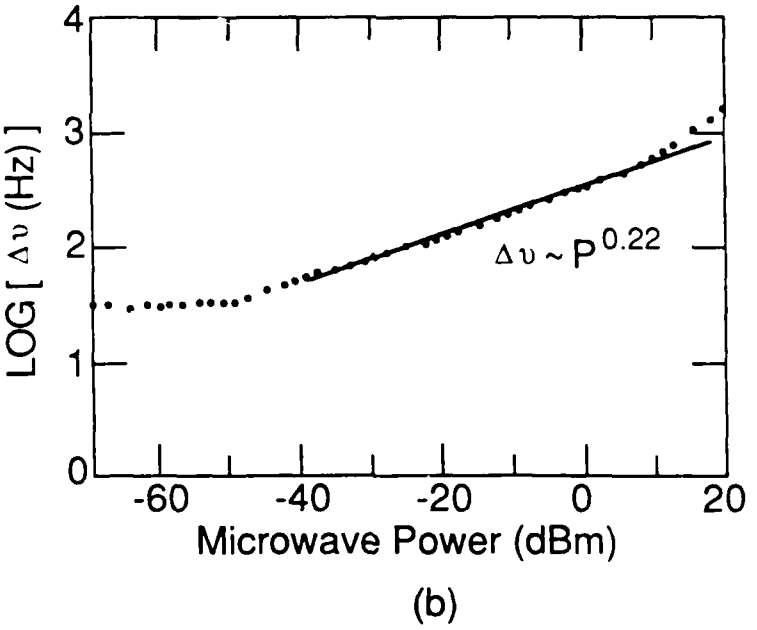

Fig. 3. Log of Clock Signal (a), and Full Width at Half-Maximum (b), as a Function of Microwave Power. For the same calculation as Fig. 2, the numerical data are again fit to power laws to determine the exponents shown in the figure.

Additionally, similar calculations were performed for a minimum volume TE_{111} cavity, and a fictitious "constant" TE_{011} cavity which was taken as having no radial variation of microwave field strength (this cavity did, however, have the normal axial field variation).

To better understand the Allan deviation's dependence on microwave power, the numerical data for the Allan deviation, the total signal amplitude (i.e., the signal summed over all tubes), and the total signal linewidth are fit to simple power law formulas:

$$\sigma_y \sim P^{\alpha} \tag{3a}$$

$$S \sim P^{\beta} \tag{3b}$$

$$\Delta\nu \sim P^{\gamma} \tag{3c}$$

The goal of this exercise is to determine the power law exponents and compare them against the single-atom case. For the range of parameters considered, we find no strong dependence of these exponents on either cavity temperature or optical pumping light intensity. The exponents seem to be a sensitive function of the cavity mode, and these results are collected in Table II.

Table I: Exponents for the Power-Law Formulas: $\sigma_y \sim P^{\alpha}$, $S \sim P^{\beta}$, and $\Delta\nu \sim P^{\gamma}$.

Field Distribution	Saturation Regime		Below Saturation Regime	
	α	γ	α	β
Completely homogeneous (single-atom case)	0.05	0.50	-1.00	1.00
TE_{011} "fictitious" (no radial variation)	0.45	0.43	-0.93	0.93
TE_{011} mode	0.20	0.22	-0.93	0.94
TE_{0111} mode	0.18	0.22	-0.94	0.96

It is clear from the table that the Allan deviation's microwave power sensitivity is directly correlated with the microwave power dependence of the clock-signal amplitude and linewidth. In the low-microwave power regime (below saturation), the linewidth is essentially constant and variations in Allan deviation are dominated by changes in signal amplitude. The signal amplitude, and consequently the Allan deviation, displays essentially no difference in the power-law scaling for the various field geometries considered. Specifically, the results show nearly the same linear power dependence as the simple single-atom case discussed above. Evidently, the clock signal amplitude is fairly insensitive to the geometry of the exciting microwave field. In the saturation regime, however, where the signal amplitude has essentially attained its maximum value and variations in the Allan deviation result from changes in the signal linewidth, the various cavity modes result in different Allan deviation power-law exponents. Furthermore, it appears that as the field is varied over an increasing number of spatial dimensions, the microwave power sensitivity of the signal linewidth decreases. This result can be explained by a correlation between the linewidth power-law exponent and the number of degrees of freedom associated with the spatial movement of the signal-dominating region. For example, a completely homogeneous field can be said to have no degrees of freedom, whereas the field of the TE_{011} mode can be said to have two degrees of freedom which are associated with movement both axially and radially. As evidenced by the results for the TE_{011} and TE_{111} cavity modes, there might be some objection to the general validity of this statement, since the TE_{111} mode has an additional angular field variation, yet shows the same signal linewidth power-law scaling as the TE_{011} mode. However, as discusssed in Section IV, for the TE_{111} mode the transverse movement of the spatial region that dominates the clock signal is limited to the radial direction. Thus, even though the field of the TE_{111} mode varies angularly, the spatial region which dominates the clock signal does not take advantage of the added degree of freedom.

As a final point we note that Fig. 2 shows a break in the power-law scaling of the Allan deviation at approximately 10 dBm, which is reflected in the linewidth data of Fig. 3b. It appears that, at these high microwave power levels, the power law exponent increases to a value near 0.4. A similar break at high microwave power levels was also seen in the TE_{111} mode calculations. Tentatively, we attribute this increase in the power law exponent to a spatial saturation of the clock-signal-dominating region; that is, the region that dominates the clock signal may not move very much for these high microwave powers. Consequently, the power law scaling takes on more of the characterisitics of the constant-field case. Further calculations, however, need to be performed to substantiate this hypothesis.

The results from these calculations thus support the general conclusion that short-term stability can be improved by varying the microwave power fed into the cavity. Specifically, since clock signal amplitudes are maximized with operation in the saturation regime, it is likely that, for a typical clock, one would want to reduce the microwave power to the point where saturation had just set in. The results, however, show that in the saturation regime the short-term stability is less sensitive to microwave power than had been previously calculated [1]; this is due to the more accurate treatment of the microwave field variation in the three-dimensional model. Consequently, order of magnitude changes in the microwave power might be required before any appreciable change in the short-term stability could be detected.

IV. INHOMOGENEITY AND POSITION SHIFT OF THE CLOCK SIGNAL VOLUME

As previously discussed, in the typical gas-cell standard a buffer gas in the clock's resonance cell effectively freezes the atoms in place. Therefore, individual atoms experience different optical and microwave field strengths, and hence contribute to the total clock signal to varying degrees. Consequently, it is common practice to imagine the clock signal as being dominated by a small spatial region in the resonance cell (i.e., the resonance cell volume is inhomogeneous with regard to its efficiency in producing clock signal), and for the clock resonance frequency to be dominated by the perturbations experienced by the atoms in this localized region. If clock parameters were to change in such a way as to shift the position of this dominant region, then the possibly different local perturbations of the new region would result in a change in clock frequency. This is referred to as the position-shift effect [12], which is considered to be a likely cause of frequency drift in the Rb standard [4].

To better understand the position-shift effect, and also to prepare for a theoretical investigation of the viability of the position shift as a mechanism of frequency drift, we have used the three-dimensional clock model to map the regions in the clock cavity that show different degrees of efficiency for producing clock signal. As illustrated in Fig. 1a, the clock cavity is imagined as being composed of hundreds of tubes: each tube transmits some small fraction of the total optical power reaching the clock photocell, and contributes to the total clock signal according to the change in optical power transmitted by the tube as the microwave frequency is varied. Since in our model different tubes can have different cross sectional areas, the efficiency of the various tubes in producing clock signal is compared by examining an individual tube's change in optical intensity (power per area). Tubes that produce the same light-intensity change as the microwave frequency is varied are then said to be "isoefficient," and in this way we have been able to establish isoefficiency contours for producing clock signal.

Fig. 4 is an example of isoefficiency contours for a cross sectional slice of a TE_{111} microwave cavity excited by -50 dBm (cavity Q = 100). The region bounded by the innermost contour corresponds to the 90th percentile efficiency region (i.e., tubes within this region exhibit a transmitted intensity change that is greater than or equal to 90% of the intensity change exhibited by the most efficient tube), the region bounded the middle contour corresponds to the 50th percentile efficiency region, and the outermost contour corresponds to the 10th percentile efficiency region. Other quantities associated with these contours are collected in Table III. In particular, the table shows that over 60% of the clock signal comes from roughly only 25% of the cavity volume.

Table III. Characteristics of Regions Bounded by Isoefficiency Contours.

Region	Fractional contribution to total signal	Fractional cavity volume occupied
90th percentile	14.1 %	4.5 %
50th percentile	62.8 %	26.3 %
10th percentile	96.8 %	66.0 %

Actually, this 60% of total clock signal is coming from less than 25% of the cavity volume, since not all axial regions of the cavity contribute to the clock signal to the same degree. The axial variation of the signal-producing efficiency is included in the calculations by modeling the axial distribution of hyperfine polarization and the axial variation of the microwave magnetic field strength, and then numerically integrating the transmitted light intensity over the length of the resonance cell. The result of the numerical integration is a significant improvement in the speed of the calculations. Simultaneously, however, there is a reduction in the facility with which

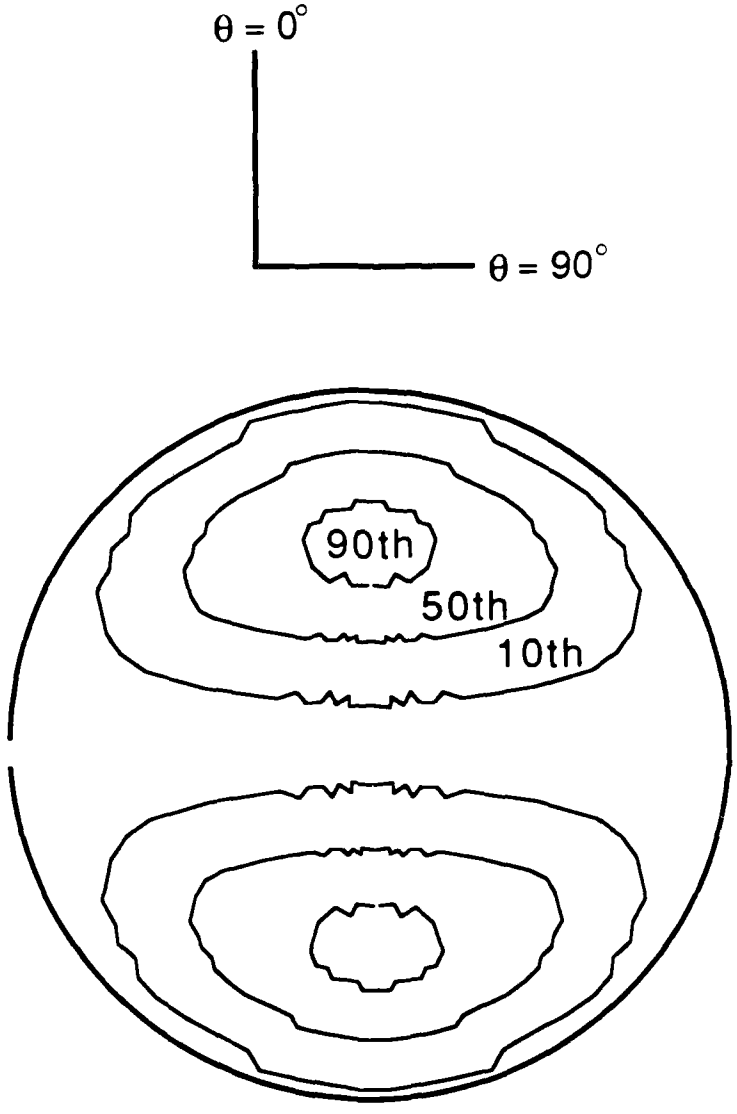

Fig. 4. Isoefficiency Contours for Producing Clock Signal. The figure shows a cross sectional slice of a TE_{111} cavity mode excited by -50 dBm (Q=100). The region bounded by the innermost contour is the 90th percentile region for efficiently producing clock signal as discussed in the text. Essentially, the 90th percentile region is more efficient than the 50th percentile region in producing clock signal, which in turn is more efficient than the 10th percentile region.

spatial information in the axial dimension may be obtained. Consequently, at the present time we can only say that the 25% is an upper bound to the volume, though we do not expect its true value to differ by more than a factor of about 2.

Considering the inhomogeneous nature of the signal volume discussed above, and how one typically imagines the clock signal as being dominated by a small spatial region within the clock cavity, we see that the three-dimensional model provides some justification for this simple description, but it does not completely validate it. The model does show that the clock signal derives from a localized spatial region within the clock cavity, but it also shows that this spatial region corresponds to a nonnegligible fraction of the cavity volume. With the simple description of the signal volume as being dominated by a small region, there is the implication that the perturbations determining the clock's frequency are fairly well localized; this, however, is not substantiated by the three-dimensional model. Considering Fig. 4 and Table III, it is more accurate to state that the clock's frequency offset from some nominal frequency corresponds to a weighted average of perturbations over a fraction of the cavity volume.

The isoefficiency contours can also be used to illustrate the fashion in which the position-shift effect occurs. Fig. 5 shows 90th percentile isoefficiency contours for input microwave powers of -50 dBm, -30 dBm and -10 dBm. Note that, as the microwave power is increased, the 90th percentile isoefficiency contour shows a macroscopic change in its position in the cavity, moving to the central region of the cavity where the hyperfine polarization is largest. If the atoms in these spatial regions were perturbed to different degrees, then there would be an atomic clock frequency change. Consequently, once the three-dimensional model incorporates spatially varying perturbations (e.g., static magnetic fields with gradients), it should be possible to launch a comprenensive theoretical investigation into the position-shift effect. Such an investigation would serve the purpose of guiding experimental research into drift, thus making the experimental effort more efficient.

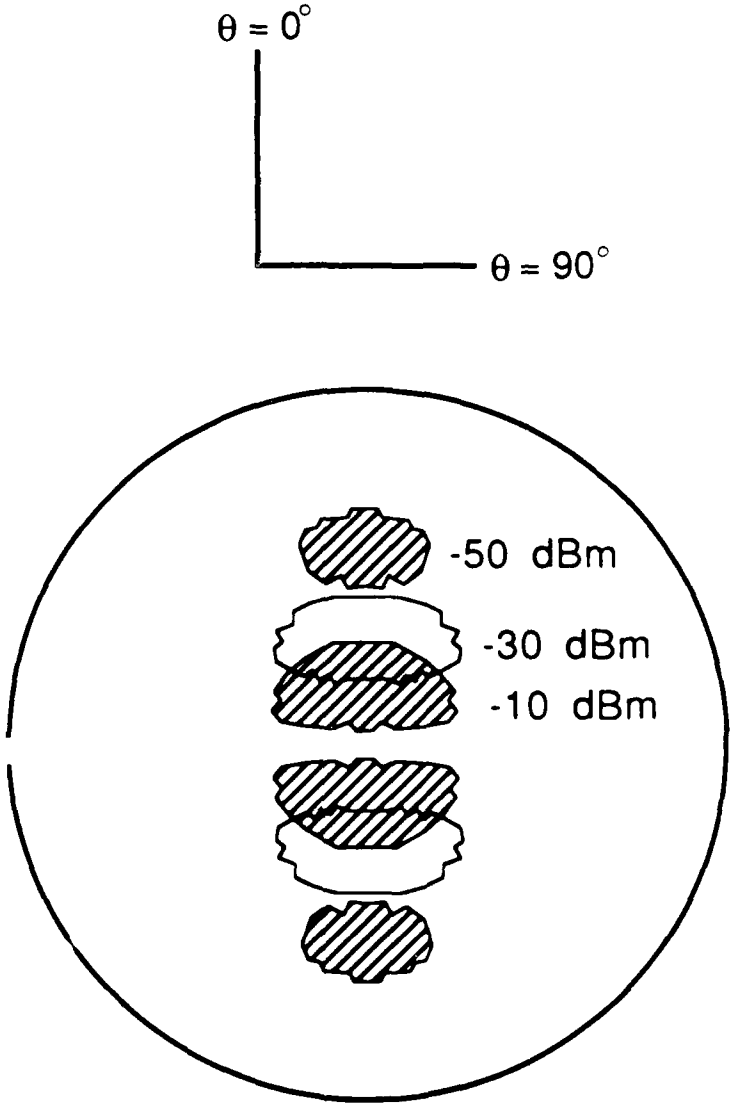

Fig. 5. Isoefficiency Contours Illustrating the Position-Shift Effect. The figure shows a cross sectional slice of a TE_{111} cavity mode (Q = 100), and the 90th percentile efficiency regions as the microwave power exciting the cavity is varied. As the microwave power is increased, the 90th percentile region shifts toward the center of the cavity. If the atoms in these different regions experienced different perturbations (i.e., different static magnetic field strengths), then the clock frequency would shift.

V. SUMMARY

We have developed a three-dimensional model of the gas-cell atomic frequency standard based on our previous one-dimensional clock model, and we are in the process of exploring its capabilities. Results presented here show that the Allan deviation's dependence on microwave power can be reasonably well modeled by power-law formulas both below and above the clock-signal saturation regime. Additionally, isoefficiency contours can be calculated and used to examine the change in position of the clock signal volume within the microwave cavity. In the near future we plan to incorporate spatially varying perturbations to the microscopic signals, and in this way to calculate atomic clock frequency shifts.

REFERENCES

[1] J. C. Camparo and R. P. Frueholz, "A nonempirical model of the gas-cell atomic frequency standard," J. Appl. Phys. 59 (2), 301 (1986).

[2] J. C. Camparo and R. P. Frueholz, "Fundamental stability limits for the diode-laser-pumped rubidium atomic frequency standard," J. Appl. Phys. 59 (10), 3313 (1986).

[3] J. C. Camparo and R. P. Frueholz, "A comparison of various alkali gas cell atomic frequency standards," IEEE Trans. Ultrason. Ferroelectrics and Freq. Control, UFFC-34 (6), 607 (1987).

[4] J. C. Camparo, "A partial analysis of drift in the rubidium gas cell atomic frequency standard," Proceeding of the 18th Annual Precise Time and Time Interval (PTTI) Applications and Planning Meeting, 1986.

[5] P. Minguzzi, F. Strumia and P. Violino, "Temperature effects in the relaxation of optically oriented alkali vapors," Nuovo Cimento 46B (2), 145 (1966).

[6] P. Tremblay, N. Cyr, and M. Tetu, "Pumping light intensity transmitted through an inhomogeneously broadened line system: application to passive rubidium frequency standards," Can. J. Phys. 63 (12), 1563 (1985).

[7] H. E. Williams, T. M. Kwon and T. McClelland, "Compact rectangular cavity for rubidium vapor cell frequency standards," Proceeding of the 37th Frequency Control Symposium (IEEE, New York, 1983), 12-17.

[8] J. Vanier and L.-G. Bernier, "On the signal-to-noise ratio and short-term stability of passive rubidium frequency standards," IEEE Trans. Instrum. Meas. IM-30 (4), 277 (1981).

[9] T. McClelland, L. K. Lam and T. M. Kwon, "Anomalous narrowing of magnetic-resonance linewidths in optically pumped alkali-metal vapors," Phys. Rev. A 33 (3), 1697 (1986).

[10] See for example the results in: I. Matsuda, N. Kuramochi, N. Shiomi and H. Fukuyo, "Signal intensity characteristics of the ^{87}Rb double resonance due to the pumping light," Jap. J. Appl. Phys. 16 (3), 391-396 (1977).

[11] R. P. Frueholz and J. C. Camparo, "Microwave field strength measurement in a rubidium clock cavity via adiabatic rapid passage," J. Appl. Phys. 57 (3), 704 (1985).

[12] A. Risley and G. Busca, "Effect of line inhomogeneity on the frequency of passive Rb_{87} frequency standards," Proceedings of the 32nd Annual

Frequency Control Symposium (Electronics Industries Association, Washington DC, 1978) 506-513; A. Risley, S. Jarvis and J. Vanier, "The dependence of frequency upon microwave power of wall-coated and buffer-gas-filled gas cell Rb_{87} frequency standards," J. Appl. Phys. 51 (9), 4571 (1980).

LABORATORY OPERATIONS

The Aerospace Corporation functions as an "architect-engineer" for national security projects, specializing in advanced military space systems. Providing research support, the corporation's Laboratory Operations conducts experimental and theoretical investigations that focus on the application of scientific and technical advances to such systems. Vital to the success of these investigations is the technical staff's wide-ranging expertise and its ability to stay current with new developments. This expertise is enhanced by a research program aimed at dealing with the many problems associated with rapidly evolving space systems. Contributing their capabilities to the research effort are these individual laboratories:

Aerophysics Laboratory: Launch vehicle and reentry fluid mechanics, heat transfer and flight dynamics; chemical and electric propulsion, propellant chemistry, chemical dynamics, environmental chemistry, trace detection; spacecraft structural mechanics, contamination, thermal and structural control; high temperature thermomechanics, gas kinetics and radiation; cw and pulsed chemical and excimer laser development including chemical kinetics, spectroscopy, optical resonators, beam control, atmospheric propagation, laser effects and countermeasures.

Chemistry and Physics Laboratory: Atmospheric chemical reactions, atmospheric optics, light scattering, state-specific chemical reactions and radiative signatures of missile plumes, sensor out-of-field-of-view rejection, applied laser spectroscopy, laser chemistry, laser optoelectronics, solar cell physics, battery electrochemistry, space vacuum and radiation effects on materials, lubrication and surface phenomena, thermionic emission, photosensitive materials and detectors, atomic frequency standards, and environmental chemistry.

Computer Science Laboratory: Program verification, program translation, performance-sensitive system design, distributed architectures for spaceborne computers, fault-tolerant computer systems, artificial intelligence, microelectronics applications, communication protocols, and computer security.

Electronics Research Laboratory: Microelectronics, solid-state device physics, compound semiconductors, radiation hardening; electro-optics, quantum electronics, solid-state lasers, optical propagation and communications; microwave semiconductor devices, microwave/millimeter wave measurements, diagnostics and radiometry, microwave/millimeter wave thermionic devices; atomic time and frequency standards; antennas, rf systems, electromagnetic propagation phenomena, space communication systems.

Materials Sciences Laboratory: Development of new materials: metals, alloys, ceramics, polymers and their composites, and new forms of carbon; nondestructive evaluation, component failure analysis and reliability; fracture mechanics and stress corrosion; analysis and evaluation of materials at cryogenic and elevated temperatures as well as in space and enemy-induced environments.

Space Sciences Laboratory: Magnetospheric, auroral and cosmic ray physics, wave-particle interactions, magnetospheric plasma waves; atmospheric and ionospheric physics, density and composition of the upper atmosphere, remote sensing using atmospheric radiation; solar physics, infrared astronomy, infrared signature analysis; effects of solar activity, magnetic storms and nuclear explosions on the earth's atmosphere, ionosphere and magnetosphere, effects of electromagnetic and particulate radiations on space systems; space instrumentation.

END

DATE

FILMED

DTIC

JULY 88